

Photostability and Skin Penetration of Different *E*-Resveratrol-Loaded Supramolecular Structures

Cassia Britto Detoni¹, Gabriele Dadalt Souto², Ana Luiza Maurer da Silva¹, Adriana Raffin Pohlmann^{1,3} and Sílvia Stanisuaski Guterres*^{1,2}

¹Programa de Pós-graduação em Ciências Farmacêuticas, Universidade Federal do Rio Grande do Sul, Porto Alegre, RS, Brazil

²Programa de Pós-Graduação em Nanotecnologia Farmacêutica, Universidade Federal do Rio Grande do Sul, Porto Alegre, RS, Brazil

³Departamento de Química Orgânica, Instituto de Química, Universidade Federal do Rio Grande do Sul, Porto Alegre, RS, Brazil

Received 16 November 2011, accepted 15 March 2012, DOI: 10.1111/j.1751-1097.2012.01147.x

ABSTRACT

It is desirable and challenging to prevent *E*-resveratrol (*E*-RSV) from photoisomerizing to its *Z*-configuration to preserve its biological and pharmacological activities. The aim of this research was to evaluate the photostability of *E*-RSV-loaded supramolecular structures and the skin penetration profile of chemically and physically stable nanostructured formulations. Different supramolecular structures were developed to act as carriers for *E*-RSV, that is, liposomes, polymeric lipid-core nanocapsules and nanospheres and solid lipid nanoparticles. The degrees of photostability of these formulations were compared with that of an ethanolic solution of *E*-RSV. The skin penetration profiles of the stable formulations were obtained using vertical diffusion cells (protected from light and under UVA radiation) with porcine skin as the membrane, followed by tape stripping and separation of the viable epidermis and dermis in a heated water bath. Photoisomerization was significantly delayed by the association of resveratrol with the nanocarriers independently of the supramolecular structure. Liposomes were the particles capable of maintaining *E*-RSV concentration for the longest time. On the other hand, *E*-RSV-loaded liposomes reduced in size showing low physical stability under UVA radiation. In the dark, the skin penetration profiles were very similar, but under UVA radiation the *E*-RSV-loaded nanocarriers showed increasing amounts in the total epidermis.

INTRODUCTION

Resveratrol (RSV; 3,5,4-trihydroxystilbene) is a naturally occurring nonflavonoid polyphenolic compound presenting *Z*- and *E*-isomeric forms (1,2). This substance has received considerable interest from the scientific community in recent years as a potential chemopreventive agent for skin cancer (3). Studies have shown that topical application of *E*-resveratrol (*E*-RSV) can prevent *in vivo* UV-induced skin damage and chemical-induced skin cancer (4–6). An *in vitro* study also

indicated that *E*-RSV is capable of treating melanoma by inducing cellular apoptosis (7).

Topical application is a route of administration that greatly exposes the formulation to sunlight and unfortunately *E*-RSV is susceptible to UV-induced isomerization, and it is almost completely converted to the less active *Z* conformation by UVA radiation (1). Studies on the structure-activity relationship of *E*-RSV show that the presence of a hydroxyl group at position 4 (4-OH), as well as the *E* stereoisomer configuration, are required for the inhibition of cell proliferation and a high antioxidant activity (2). Thus, it is worthwhile and challenging to prevent RSV from isomerizing to preserve its biological and pharmacological activities.

Recently, nanocapsules have been proposed as a strategy to overcome inactivation and/or degradation of photosensitive drugs (8–11). The materials and designs used to build nanostructures capable of protecting biologically active molecules from light vary immensely. Among the possibilities for nanostructured carriers there is a preference for those prepared with biodegradable materials such as lipids or biodegradable polymers. The supramolecular structures of nanoparticles may vary, having a compartmented structure (core and wall) or a matrix structure (12). Of the biodegradable nanostructured carriers described to date, the most studied supramolecular structures are the polymeric nanoparticles (nanocapsules and nanospheres), lipid nanoparticles and liposomes (13,14).

Polymeric nanoparticles are known to stabilize photolabile drugs by providing physical protection from UV radiation (8). The particles containing a mixture of medium-chain triglycerides and sorbitan monostearate in their core, named lipid-core nanocapsules, have exhibited the properties of great stability and high drug association efficiency for different drugs intended for administration by various routes (15). Indeed, lipid-core nanocapsules have exhibited a good photostabilization capacity for the sunscreens octyl methoxycinnamate and benzophenone-3 as well as the polyphenol quercetin (8,16). Furthermore, the proposed *E*-RSV lipid-core nanocapsules have already proven their pharmacological potential, by exhibiting higher gastrointestinal safety and better tissue distribution after oral administration than free *E*-RSV (17).

*Corresponding author email: silvia.guterres@ufrgs.br (Sílvia Stanisuaski Guterres)

© 2012 Wiley Periodicals, Inc.

Photochemistry and Photobiology © 2012 The American Society of Photobiology 0031-8655/12

Other lipid-based nanoparticles are also capable of photostabilizing drugs. For instance, liposomes are an extensively studied photoprotective carrier system and successful results have been reported in many studies (11,18). Phosphatidylcholine liposomes have been applied as a vehicle for tretinoin, increasing its photostability and reducing its photoisomerization. The results indicated that higher drug inclusion in liposomes leads to a higher photostabilization (11). Solid lipid nanoparticles and nanostructured lipid carriers have appeared as an alternative to liposomes due to improved physical stability and low cost compared with phospholipids (19) and have also been successfully used to photostabilize tretinoin (20). Lipid-based nanoparticles may be prepared using the high-pressure homogenization technique, which allows the pharmaceutical industry to obtain liposomes and nanostructured lipid carriers in large-scale production (19,21).

Besides maintaining the chemical stability of *E*-RSV in the formulation, nanostructured formulations intended for cutaneous administration should guarantee its physical stability following UVA radiation, in terms of mean particle size and size distribution. Among the chosen carriers, liposomes present the most dynamic behavior and therefore they are, theoretically, the least physically stable. On the other hand, polymeric nanoparticles are known for their high structural stability (22), and these carriers are frequently preferred due to this characteristic. Solid lipid nanoparticles and nanostructured lipid carriers have been developed aiming to aggregate the benefits of a lipid structure with higher physical stability (19). Another characteristic that leads to difficulties in relation to the topical application of *E*-RSV is that in its nonionized form (pH 5.0–8.0) this drug has a high permeation and penetration capacity, although this facilitates its transdermal application (23). By increasing the retention of *E*-RSV in the upper layers of the skin it is possible to increase its topical activity, reducing loss to the systemic circulation. In this regard, nanocarriers may improve the skin retention of substances that are designed to act at the upper layers of the skin, such as sunscreens, antioxidants and repellents (24,25). A topical chemopreventive active compound should mostly act in the various layers of the epidermis where UVA absorption is higher and where most mutagenesis occurs (26).

Resveratrol skin administration has been tested in different hydrogel matrices at a concentration of 5% and the highest permeability coefficient was observed using hydroxyethyl cellulose (23). The topical administration of RSV in nanocarriers has been previously proposed in liposomes and solid lipid nanocarriers viewing improved chemotherapeutic and chemopreventive activities (27,28).

Even though polymer based and lipid nanoparticles have the potential to protect drugs from photoreactions it is unknown which kind of supramolecular structure protects sensitive drugs the most. Taking these considerations into account, the objective of this study was to prepare different *E*-RSV-loaded supramolecular structures with a variety of materials and architectures, to compare the photostabilizing capacity of the different structures. Thus, two lipid-based carriers, liposomes and nanostructured lipid carriers (NLC), as well as two polymer based structures, lipid-core nanocapsules and nanospheres, were studied as potential photostability enhancers for *E*-RSV. In addition, the skin penetration

profile of a chemically and physically stable *E*-RSV-loaded colloidal formulation was evaluated and compared with that of the free molecule, aiming at its retention in the upper layers of the skin.

MATERIALS AND METHODS

Solvents and reagents. Saturated soy phosphatidylcholine S 75-3 was donated by Lipoid (Ludwigshafen, Germany). Lipid glyceryl dibehenate (Compritol 888[®]) was purchased from Brasquim (Porto Alegre, Brazil); coconut fat, medium-chain triglycerides and *E*-RSV were from Cosmetrade (Porto Alegre, Brazil); sorbitan monooleate from Oxiteno (Mauá, SP, Brazil) and polysorbate 80 from Vetec (Rio de Janeiro, Brazil). Poly (ϵ -caprolactone; $M_w = 65\,000\text{ g}\cdot\text{mol}^{-1}$) and sorbitan monooleate were acquired from Sigma–Aldrich (Steinheim, Germany). The analytical grade solvent chloroform was purchased from Labsynth (Diadema, Brazil) and acetone from F. Maia (Cotia, Brazil). The high-performance liquid chromatography (HPLC) grade solvents acetonitrile and ethanol were obtained from Tedia (Rio de Janeiro, Brazil).

Particle preparation. Initially, lipid-core nanocapsules, nanospheres, liposomes and NLC containing *E*-RSV were prepared. The polymeric particles were obtained through the precipitation of a preformed polymer. Briefly, a water miscible organic solvent, in this case acetone, containing the hydrophobic components was slowly injected into the aqueous phase containing a hydrophilic surfactant, followed by solvent elimination under vacuum evaporation at moderate rotation (Büchi R 114). The volumes of the two phases were 67.5 mL of organic phase and 132.5 mL of aqueous phase. The final volume, after evaporation, was 25 mL. The formulation contained the hydrophobic components; poly(ϵ -caprolactone; $10\text{ mg}\cdot\text{mL}^{-1}$), sorbitan monooleate ($3.8\text{ mg}\cdot\text{mL}^{-1}$), *E*-RSV ($1\text{ mg}\cdot\text{mL}^{-1}$) and, in the case of the lipid-core nanocapsules, medium-chain triglycerides ($33\text{ mg}\cdot\text{mL}^{-1}$). The aqueous phase of the formulation contained polysorbate 80 ($3.8\text{ mg}\cdot\text{mL}^{-1}$).

The lipid-core nanocapsule formulation using poly (ϵ -caprolactone) was based on a previous study (17). To prepare nanosphere the same materials and proportion were used, except for the liquid oil (medium-chain triglycerides) that is absent. In addition, these compositions were equal or very similar to those described in various previous articles (8–10,12,13,15,16).

Liposomes were prepared by the thin lipid film hydration method followed by high-pressure homogenization (Panda 2K NS1001L, GEA Niro Soavi). Saturated soy phosphatidylcholine was dissolved with *E*-RSV ($1\text{ mg}\cdot\text{mL}^{-1}$) in a mixture of chloroform:methanol (75:25) and evaporated under reduced pressure. The lipid film was hydrated with distilled water under sonication. The suspension was then homogenized by high-pressure homogenization. Variations of phosphatidylcholine concentration (1.6 and $3.2\text{ mg}\cdot\text{mL}^{-1}$), homogenization pressure (180 and 250 bar) and number of cycles (6 and 10) were tested to obtain a nanosized formulation. The final formulation was chosen based on the particle size distribution.

The NLC were also prepared by high-pressure homogenization (Panda 2K NS1001L, GEA Niro Soavi) that followed a pre-emulsion process at high temperature (70°C). In the hydrophobic phase, the solid lipids Compritol 888[®] (Brasquim; $10\text{ mg}\cdot\text{mL}^{-1}$) and coconut fat (0 and $6\text{ mg}\cdot\text{mL}^{-1}$) were used. Medium-chain triglycerides (26 and $20\text{ mg}\cdot\text{mL}^{-1}$), sorbitan monooleate ($3.8\text{ mg}\cdot\text{mL}^{-1}$) and *E*-RSV ($1.0\text{ mg}\cdot\text{mL}^{-1}$) were added to the hydrophobic phase which was melted at 70°C . The aqueous phase contained $3.8\text{ mg}\cdot\text{mL}^{-1}$ of polysorbate 80 and was added to the hydrophobic phase to form a pre-emulsion that was prepared with an UltraTurrax[®] (24 000 rpm; IKA[®] Works, Inc. São Paulo, Brazil) prior to the high-pressure homogenization. Variations of coconut oil and medium-chain triglycerides concentration as well as number of cycles (three and six) were used as preliminary tests to produce a nanosized formulation.

Drug content and association efficiency. The drug content and association efficiency were determined by a validated HPLC. The developed method was based on a method previously used by Sapino *et al.* (1). A solution of methanol:water (1:1, vol/vol) at pH 3.0, adjusted with acetic acid, was used as mobile phase. The column used was a Luna 5 μ C18 (2) 100 Å with size of $150 \times 4.60\text{ mm}$ (Phenomenex[®], Torrance, CA). The mobile phase flow was $0.6\text{ mL}\cdot\text{min}^{-1}$,

wavelength 305 nm and the volume of sample injected was 20 μL . The method had a squared correlation coefficient (R^2) of 0.999 in the range of 1–20 $\mu\text{g}\cdot\text{mL}^{-1}$, was precise (with relative standard deviations [SDs] under 4.0% for all formulations) and accurate (with a recovery of 95–105% for all formulations). This method is capable of separating *E*- and *Z*-isomers and the retention times are 6.2 and 9.5 min, respectively. The drug content was determined by adding *E*-RSV loaded formulations to methanol followed by 5 min of ultrasonication, filtration and quantitation. To determine the association efficiency, free *E*-RSV was separated from the particles by ultrafiltration centrifugation (Ultrafree-MC 10 000 MW, Merk Millipore, Darmstadt, Germany) at 5000 rpm for 10 min at 20°C and the free *E*-RSV was quantified.

Particle size distribution. The particle *z*-average (diameter) and polydispersity index were determined by dynamic light scattering (Zetasizer Nanoseries; Malvern Instruments, Worcestershire, UK) at an angle of 173°. Twenty microliters of the samples was added to 10 mL of Milli Q® water and transferred to polystyrene cuvettes for each analysis.

Transmission electron microscopy. The morphological aspect of the particles was evaluated by transmission electron microscopy (TEM; Jeol, JEM 1200 Exll, Centro de Microscopia Eletrônica-UFGRS) operating at 120 kV. The diluted suspensions were deposited on formvar-carbon supported on copper grids (Electron Microscopy Sciences). The samples were negatively stained with a uranyl acetate solution (2% m/vol).

Particle concentration. The number of particles per milliliter was estimated by turbidimetry according to the method described by Zattoni *et al.* (29). Briefly, the samples were diluted with MilliQ® water to give five different concentrations that presented absorbance values between 0.2 and 1.0 and analyzed at the wavelength 590 nm (where there is no absorption). The number of particles was calculated from the absorbance, diameter and density values.

***E*-RSV photostability assay.** The photostability assay was performed by irradiating the samples in a mirrored chamber with a UVA light source ($<1\text{ mW}\cdot\text{cm}^{-2}$). Samples were placed in polystyrene cuvettes with a 20 cm distance from the light source and the experiment was carried out in triplicate for each sample (liposomes, lipid-core nanocapsules, nanospheres and NLC). All formulations were aqueous suspension and the control (free *E*-RSV) was an ethanol solution. This solvent was chosen because *E*-RSV presents high solubility in ethanol. Furthermore, ethanol presents a protective effect on the photodegradation of *E*-RSV if compared with water (medium of the tested formulations), as cited by Sapino *et al.* (1), assuring that the solvent is not responsible for the extent of degradation of the free *E*-RSV. Degradation was verified by UV spectroscopy following the method described by Camont *et al.* (30), this method was compared to the HPLC method described earlier in this article. In addition, none of the formulations' components, except RSV, absorb between 250 and 400 nm.

At determined time intervals, aliquots of 50 μL were taken from each sample and diluted to 5 mL of ethanol, homogenized, centrifuged, placed in quartz cuvettes and analyzed in a spectrophotometer. The *E*-RSV concentration was calculated at each time interval using Eq. (1) as follows:

$$C_E = \frac{1}{R-1} \cdot \left(\frac{R \cdot A}{l \cdot \varepsilon} - C_o \right) \quad (1)$$

where $R = \varepsilon_{E,305\text{ nm}}/\varepsilon_{Z,305\text{ nm}} = 3.60$ at 305 nm, C_E is the concentrations of *E*-RSV ($\mu\text{g}\cdot\text{mL}^{-1}$) at the time of the analysis, ε is the molar extinction coefficient of *E*-RSV ($\mu\text{g}\cdot\text{mL}^{-1}$), C_o is the initial concentration of *E*-RSV (before exposure), A is the measured absorbance and l is the optical path length (cm).

The molar extinction coefficient of *E*-RSV was calculated for the wavelength 305 nm and the optical path length of 1 cm, using the Lambert–Beer law (Eq. [2]),

$$A = \varepsilon_E \cdot l \cdot C \quad (2)$$

where A is the absorbance, l is the optical path length, C is the concentration and ε is the molar extinction coefficient. The molar extinction coefficient of *Z*-RSV measured after 60 min of irradiation of a *E*-RSV ethanolic solution, which was analyzed by HPLC and a UV spectrophotometer. The molar extinction coefficient of *Z*-RSV was calculated using Eq. (3):

$$\varepsilon_Z = \frac{\%A \cdot \varepsilon_E \cdot C_o}{C_Z} \quad (3)$$

where ε_E and ε_Z are the molar extinction coefficients of *E*- and *Z*-RSV, respectively, $\%A$ is the percentual area represented by *Z*-RSV in the chromatogram, C_Z is the complementary concentration of *E*-RSV obtained by the HPLC method ($C_Z = C_o - C_E$) and C_o is the initial concentration of *E*-RSV.

The degradation profile of the *E*-RSV concentration was plotted as a function of the exposure time, and modulated using first kinetic models (Eq. [4]; software MicroMath Scientist®, St. Louis, MO).

$$\ln(C) = \ln(C_o) - k_t \quad (4)$$

Physical stability of nanostructures. The physical stability of the particles was evaluated by measuring the particle size by dynamic light scattering (Zetasizer Nanoseries; Malvern Instruments) after UVA radiation under the same conditions as the chemical stability assay for 0, 120 and 720 min.

Skin penetration. A penetration assay using automated Franz cells (MicroettePlus Multi Group® Hanson Research Corporation) with a modified liquid formulation apparatus and porcine skin as a membrane was performed with the particles that presented improved chemical and physical stability, lipid-core nanocapsules and NLC. As a control a water:ethanol (6:4, vol/vol) solution of free *E*-RSV with a concentration of 1 $\text{mg}\cdot\text{mL}^{-1}$ was used. A volume of 0.2 mL was applied on the skin surface for all samples. The receptor medium was water with 2% of polysorbate 80, ensuring sink condition during the entire experiment, at a temperature of $32 \pm 2^\circ\text{C}$ and constant stirring at 400 rpm. The porcine skin, obtained from a slaughterhouse (Frigorífico Porto Ijuí, Brazil), was comprised of total epidermis and dermis. The skin was reduced to a width of 2.0 ± 0.15 mm, cleaned with sodium lauryl sulfate aqueous solution (1%) on the internal surface and with ether on the external surface. The area of the exposed skin was 1.76 cm^2 .

After 8 h the experiment was ended, the stratum corneum was separated by the tape stripping technique with 18 tapes (Scotch tape 3M®, Sumaré, Brazil) and the viable epidermis and dermis were separated by heating the skin in a water bath at 60°C for 45 s and separating the epidermis with a spatula. *E*-RSV was extracted from the skin layers with acetonitrile:water (3:1, vol/vol) and 1 h of sonication. The extraction recovery from skin samples using this method was $85.3 \pm 3.7\%$. *E*-RSV was quantified by the HPLC method described elsewhere. This procedure was carried out in sextuplicate, in the dark and under UVA exposure.

Statistical analysis. Data were evaluated by two-way analysis of variance (ANOVA) followed by Tukey's test (BioEstat 5.0®, Instituto de Desenvolvimento Sustentável Mamirauá, Belém, Pará, Brazil). The significance level (alpha) applied was 0.05. The values are expressed as the mean \pm standard deviation.

RESULTS

Nanocarrier preparation and characterization

Both polymeric particles had a nanometric and monomodal size distribution (266 nm for nanocapsules, 207 nm for nanospheres and PI values of 0.16 and 0.16, respectively). To prepare an adequate nanosized liposome (189 nm and PI of 0.29), phosphatidylcholine concentration was 1.6 $\text{mg}\cdot\text{mL}^{-1}$ and the process parameters were 10 cycles of homogenization at a pressure of 250 bars. The nanostructured lipid carrier formulation without coconut fat did not present a monomodal size distribution showing two particle populations (137 nm and 531 nm). The addition of coconut fat (6 $\text{mg}\cdot\text{mL}^{-1}$) and the reduction of medium-chain triglycerides from 26 to 20 $\text{mg}\cdot\text{mL}^{-1}$ resulted in a formulation with a monomodal size distribution (176 nm and PI 0.12).

A comparison among lipid-core nanocapsules (266.2 nm), nanospheres (207.1 nm) and liposomes (189.4 nm) showed

statistically similar values in terms of particle size ($P > 0.05$). The smallest z -average size was observed for the NLC (176.0 nm). The polydispersity indexes (PI) were below 0.3 for all nanostructured carriers suggesting that each preparation method led to controlled size distributions. The pH for all aqueous suspensions ranged from 5.4 to 5.9. *E*-RSV was successfully loaded in all particles and presented association efficiency of 98–100%, which is expected for hydrophobic molecules such as *E*-RSV (Table 1). TEM showed that all particles had almost spherical shapes and confirmed their nanometric size (Fig. 1).

For the lipid-core nanocapsules the results of the turbidimetry assays indicated an estimated concentration of $4.7 \pm 0.2 \times 10^{12}$ particles per mL, nanospheres of $7.6 \pm 0.2 \times 10^{12}$ particles per mL, liposomes of $6.1 \pm 0.2 \times 10^{10}$ particles per mL and NLC of $1.4 \pm 0.05 \times 10^{11}$ particles per mL.

E-RSV photostability assay

For *E*-RSV, the molar extinction coefficient at the wavelength of 305 nm was $27\,775 \text{ L}\cdot\text{mol}^{-1}\cdot\text{cm}^{-1}$ and for *Z*-RSV it was $7703 \text{ M}^{-1}\cdot\text{cm}^{-1}$. To verify that Eq. (1) was applicable under the

Table 1. Physical–chemical characteristics of the *E*-RSV loaded nanostructures. Data are presented as means \pm SD.

Particles	z -average (nm)	<i>E</i> -RSV content (%)	Association efficiency (%)	pH
Nanocapsules	266.2 ± 0.72	98.1 ± 0.19	99.6	5.85
Nanospheres	207.1 ± 8.11	102.1 ± 0.32	98.0	5.50
Liposomes	189.4 ± 14.1	100.9 ± 0.12	99.1	5.47
Nanostructured lipid carriers	176.0 ± 5.06	102.4 ± 0.12	98.4	5.89

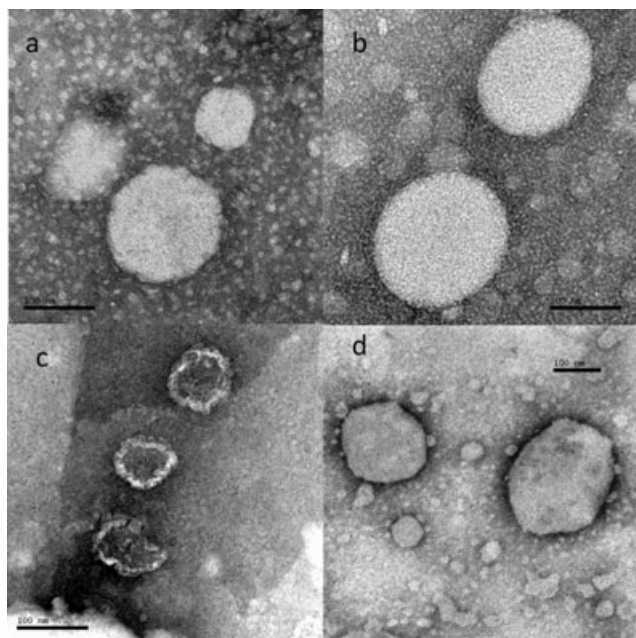


Figure 1. Transmission electron micrographs of lipid-core nanocapsules (a), nanospheres (b), liposomes (c) and nanostructured lipid carriers (d).

experimental conditions applied, a *E*-RSV solution was exposed to UVA radiation and quantified simultaneously by the validated HPLC method and the spectrophotometric method first described by Camont *et al.* (30) with four different time intervals. The results for the *E*-RSV concentration provided by the two methods were similar (Fig. 2), confirming that the methods are interchangeable.

The photodegradation profile studies showed a 90.4% decrease in the *E*-RSV concentration of the ethanolic solution in 4 h (240 min) of experiment. This photoreaction was significantly slowed down by the association of *E*-RSV with all four types of nanocarriers (Fig. 3). The liposome particles maintained the *E*-RSV concentration for the longest time, the initial concentration decreasing by only 29.3% after 4 h. Concentrations of *E*-RSV reduced to 67.2%, 77.8% and 70.0% of the initial concentration within 4 h in the case of the lipid-core nanocapsules, nanospheres and NLC, respectively.

The degradation profiles were modeled considering first- and second-order kinetics (Table 2). The first-order model was chosen as the best fit for all formulations and for the ethanolic

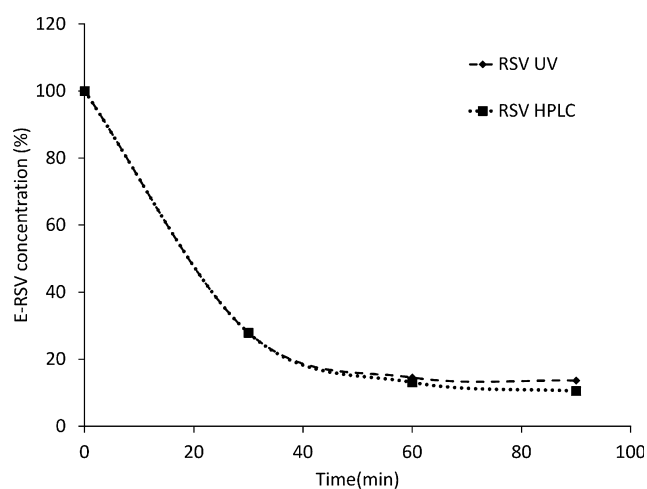


Figure 2. Degradation profile of *E*-RSV ethanol solution analyzed simultaneously by the validated HPLC method and by the spectrophotometric method first suggested by Camont *et al.* (30).

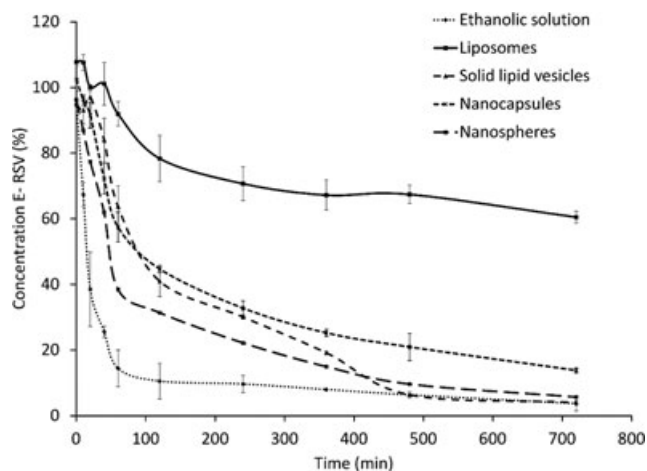


Figure 3. The photodegradation profile of *E*-RSV in ethanol solution and encapsulated in lipid-core nanocapsules, nanospheres, nanostructured lipid carriers and liposomes in aqueous suspensions.

Table 2. Kinetic parameters (coefficient R^2 , kinetic constant k , model selection criterion MSC and half-live $t_{1/2}$) of *E*-RSV photodegradation during UVA exposure for 720 min ($n = 3$). Data are presented as mean \pm SD.

Formulation	First order			
	R^2	k (min ⁻¹)	MSC	$t_{1/2}$ (min)
Ethanol solution	0.974 \pm 0.012	0.0306 \pm 0.0070	2.879 \pm 0.431	19.5 \pm 3.7
Nanocapsules	0.977 \pm 0.033	0.0057 \pm 0.00070	2.194 \pm 0.104	122.6 \pm 16.3
Nanospheres	0.975 \pm 0.008	0.0104 \pm 0.00080	2.487 \pm 0.388	67.0 \pm 5.2
Liposomes	0.988 \pm 0.003	0.00130 \pm 0.00002	1.094 \pm 0.301	592.2 \pm 9.6
Nanostructured lipid carrier	0.986 \pm 0.002	0.0051 \pm 0.00020	2.954 \pm 0.174	137.0 \pm 5.7

Table 3. Z-average diameter (SD) and polydispersity index (SD) of the nanostructured carriers after UVA radiation.

Formulation	Irradiation time (UVA)					
	0 min		120 min		720 min	
	Diameter (nm)	PI	Diameter (nm)	PI	Diameter (nm)	PI
LNC	266.2 \pm 4.1	0.16 \pm 0.02	317.7 \pm 23.3	0.15 \pm 0.05	309.3 \pm 9.9	0.13 \pm 0.02
Nanosphere	207.1 \pm 8.1	0.16 \pm 0.02	206.6 \pm 8.8	0.14 \pm 0.03	211.6 \pm 3.0	0.12 \pm 0.02
Liposomes*	189.3 \pm 14.2	0.29 \pm 0.05	216.2 \pm 25.4	0.43 \pm 0.02†	188.6 \pm 14.5	0.41 \pm 0.03†
Nanostructured lipid carriers	176.0 \pm 5.1	0.12 \pm 0.02	184.5 \pm 6.7	0.12 \pm 0.06	188.7 \pm 2.9	0.11 \pm 0.01

*bimodal size distribution profile.

solution according to the MSC and R^2 -values. All of the nanocarriers were capable of reducing the isomerization rate (K ; $P < 0.5$) of *E*-RSV. The lipid-core nanocapsules and NLC had the same degradation rate (K ; $P < 0.5$) and maintained the *E*-RSV concentration for a longer period of time than the nanospheres.

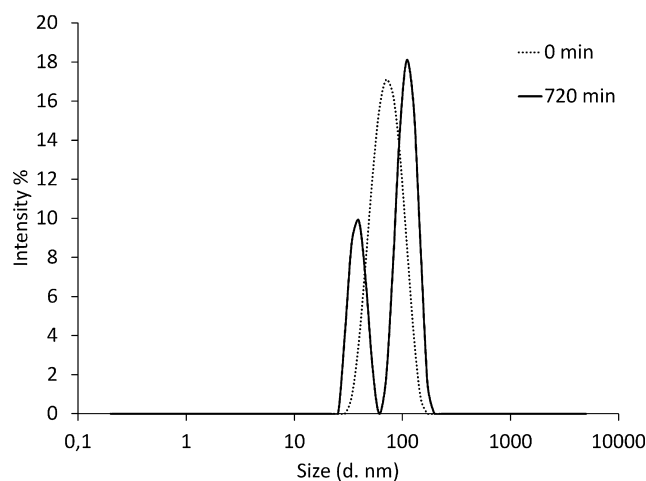
Physical stability of nanostructures

The z -average sizes of the lipid-core nanocapsules and nanospheres slightly increased upon UVA exposure, from 266.2 \pm 4.1 to 309.3 \pm 9.9 nm and from 207.1 \pm 8.1 to 211.6 \pm 3.0 nm, respectively. Although the lipid-core nanocapsules presented a greater increase in size than the nanospheres, no statistical differences between the z -average size at time zero and at 12 h ($P > 0.05$) were observed for any of the particles. The polydispersity indexes (PI) of the polymeric formulations did not vary under UVA radiation maintaining values of between 0.12 and 0.16.

After 720 min of UVA exposure the liposomes exhibited considerable fluctuations in the z -average (189.3 \pm 14.2, 216.2 \pm 25.4 and 188.6 \pm 14.5 nm) and a notable increase in the PI (from 0.29 to 0.41). NLC presented a behavior similar to the lipid-core nanocapsules and nanospheres, maintaining their original size (from 176.0 to 188.7 nm) and degree of dispersion (PI of 0.12 and 0.11; Table 3).

The liposomes assumed a dynamic and bimodal profile while all other particles remained monomodal after UVA radiation. As a consequence, the appearance of a new population of particles was observed. The mean peak diameter of the second particle population of liposomes was 86 nm (Fig. 4).

To verify the influence of *E*-RSV on the physical instability of the liposomes, liposomes formulated without *E*-RSV were evaluated under the same conditions (Fig. 5). After 8 h of

**Figure 4.** Particle size distributions obtained by PCS according to the intensity of *E*-RSV-loaded liposomes before UVA radiation and after 720 min of UVA radiation.

UVA radiation the blank liposomes presented a second population of particles with larger z -average diameters than the particles before irradiation.

Skin penetration

In the case of the particles, which presented improved *E*-RSV photostability and a constant size distribution after UVA radiation, the skin penetration was evaluated in the dark and during exposure to UVA radiation (Fig. 6).

When protected from the light, larger quantities of the free *E*-RSV penetrated into the upper layers of the skin (11.8 μ g in the stratum corneum and 23.2 μ g in the viable epidermis)

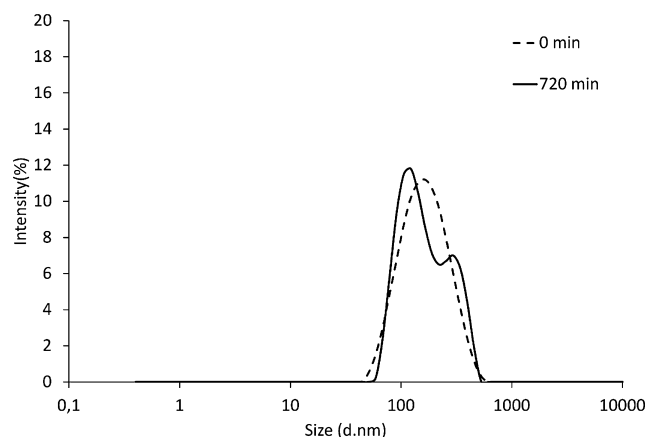


Figure 5. Particle size distribution obtained by PCS according to intensity of blank liposomes before UVA radiation and after 720 min of UVA radiation.

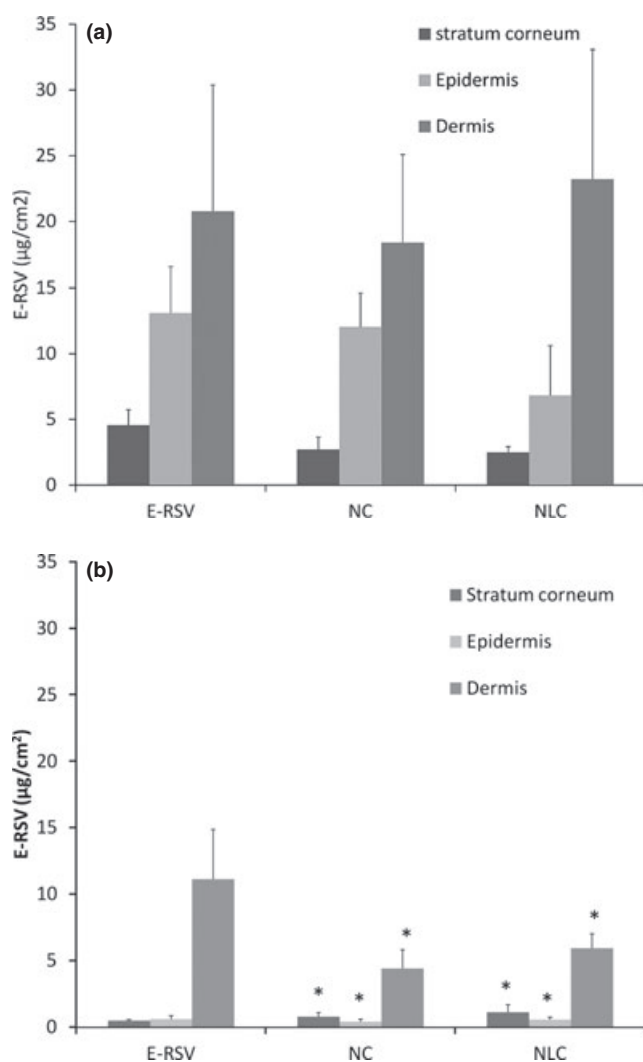


Figure 6. Skin penetration profiles of free *E-RSV*, *E-RSV*-loaded lipid-core nanocapsules and nanostructured lipid carrier in the dark (a) and exposed to UVA radiation (b). *Statistically different to the free molecule ($P < 0.05$).

compared to the *E-RSV*-loaded carriers (9.5 and 7.3 μg in the stratum corneum, 15.7 and 8.1 μg in the epidermis for lipid-core nanocapsules and nanostructured lipid carriers, respectively). Lipid-core nanocapsules showed a tendency to prevent *E-RSV* reaching the dermis (26.5 μg) when compared to the free *E-RSV* (36.8 μg) and *E-RSV*-loaded nanostructured lipid carriers (41.1 μg), although no statistically significant difference was observed.

When exposed to UVA radiation the quantities of *E-RSV* in the total epidermis (stratum corneum plus viable epidermis) were larger for lipid-core nanocapsules (2.7 μg) and for NLC (3.3 μg). In the dermis, the quantity of *E-RSV* was larger for the free molecule (17.7 μg), followed by the NLC (10.5 μg) and then lipid-core nanocapsules (7.8 μg). After 8 h of experiment none of the samples showed a quantifiable concentration of *E-RSV* in the receptor compartment.

DISCUSSION

Particle preparation and characterization

All formulations showed particle sizes consistent with the type, raw materials and preparation methods used. The nanocapsules had a z -average of 266 nm and nanospheres of 207 nm, consistent with the expected size range (200–500 nm) for polymeric formulations prepared by the method of preformed polymer precipitation (12). The liposomes had a z -average diameter of 189 nm, which is in the reported size range (80–200 nm) of nanoliposomes (31). NLC had a z -average of 176 nm in agreement with the size range (< 500 nm) described for similar formulations (32). All formulations had narrow dispersity according to the polydispersity indexes (PI), which varied from 0.11 to 0.29 (33), and these particles presented a controlled size distribution. In nanostructured systems, PI is a value used to describe the homogeneity of the particle distribution and serves as a quality control parameter. The PI of liposomes (0.29) was the highest of the formulations prepared, and for the other three types of particles this value was between 0.11 and 0.16.

The physicochemical characteristics of the particles are strongly determined by the solids concentration and volumetric fraction. As the formulations prepared required different materials and proportions, they differed in terms of particle concentration (nanocapsules $4.7 \pm 0.2 \times 10^{12}$, nanospheres $7.6 \pm 0.2 \times 10^{12}$, liposome $6.1 \pm 0.2 \times 10^{10}$ and NLC $1.4 \pm 0.05 \times 10^{11}$ particles per mL). This parameter did not appear to have a direct influence on the photostability or the isomerization rate (k) of the *E-RSV*-loaded nanocarriers, as seen in Tables 1 and 2.

The pH for all particles ranged between 5.0 and 6.0, which is acceptable considering that *E-RSV* is more photostable in the range of pH 5.0–8.0 (1). *E-RSV* presents higher skin permeation at pH values close to 6.0 (23).

Photostability assays

The association of *E-RSV* with supramolecular structures enhanced its photostability under UVA radiation, this may be observed by the increase of $t_{1/2}$ from 19.5 min to at least 67 min (Table 2). The observed differences between the associated and free RSV are probably higher than reported,

considering that ethanol may exhibit a protective effect on *E*-RSV when compared with an aqueous medium (1).

The different designs of polymeric particles resulted in nanocarriers with different photostabilizing capacities. The vesicular polymeric system of lipid-core nanocapsules was able to photostabilize *E*-RSV for a longer period of time than the nanospheres. The $t_{1/2}$ was almost twice as long for the nanocapsules (122.6 ± 16.3 min) compared with the nanospheres (67.0 ± 5.2 min).

The lipid-core nanocapsules and nanospheres were physically stable for 12 h (720 min) under UVA exposure. In a different study, a similar result was obtained with polymeric nanocapsules containing OMC and quercetin after exposure for 15 days (8). Therefore, *E*-RSV association did not influence the physical stability of the particles, which maintained PI values of 0.15 and 0.13 after 120 and 720 min, respectively.

The system in which the *E*-RSV had the highest photostability was the liposome structure, with a $t_{1/2}$ of 592.2 ± 9.6 min. In our study, the lipophilic characteristic of *E*-RSV and the high association efficiency of the *E*-RSV liposomes indicate that the molecules are probably imbibed in the phospholipid bilayer, leading to a high photostabilization. Phosphatidylcholine degradation may lead to UVA absorption (34), which would result in erroneous results for the determination of the *E*-RSV concentration by the method used herein. For this reason, the UV absorption of a blank formulation was monitored during UVA exposure for the experimental period and no absorption was observed at between 250 and 400 nm.

Liposomes were not physically stable during exposure to UVA radiation, in the case of both drug loaded and blank vesicles. Liposomes assumed a dynamic and bimodal profile. A second population of larger particles appeared in the blank formulation, probably as a result of the phenomena of fusion and/or agglomeration due to the high energy "input" during UVA radiation. For the liposomes containing *E*-RSV, a second population of smaller particles appeared after 8 h of UVA radiation. The appearance of smaller particles was attributed to a disruption of the vesicle into smaller fragments due to the *E*-*Z* isomerization of the RSV imbibed in the bilayer. The disruption of the vesicle into smaller fragments is well described for phosphatidylcholines with azobenzene groups (35). When comparing the molecular structure of azobenzene and RSV we noted that the basic skeleton of the molecules is the same, and that RSV has a hydroxyl group on each aromatic ring. It is possible that the linear structure of *E*-RSV favored the liposome bilayer stability, and that on isomerizing to *Z*-RSV the molecule loses its linear configuration and the vesicle breaks (Fig. 7).

The NLC had statistically the same isomerization rate (K) and $t_{1/2}$ as the lipid-core nanocapsules, with $t_{1/2}$ values of 122.6 ± 16.3 and 137.0 ± 5.7 min, respectively. These two types of particles were formulated to have similar solids concentrations, $0.041 \text{ g}\cdot\text{mL}^{-1}$ for NLC and $0.048 \text{ g}\cdot\text{mL}^{-1}$ for lipid-core nanocapsules, and the liquid lipid used was also the same (medium-chain triglycerides). The similarities in terms of composition may have contributed to similarities in the photoisomerization profile.

Nanostructured lipid carriers presented physical stability after UVA exposure. The monomodal profile with a polydispersion index of 0.12 ± 0.02 was maintained over 12 h. Due

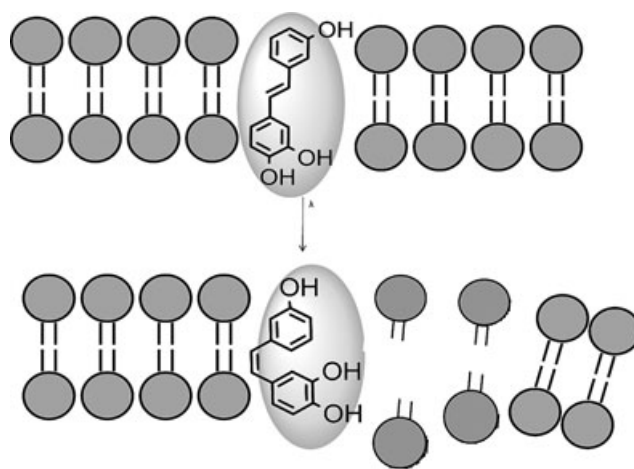


Figure 7. Illustration of resveratrol *E*-*Z* isomerization in the bilayer membrane leading to fragmentation of the vesicle.

to the lipid nature, this nanostructure may present morphological variations after an increase in temperature or a high energy input, exposure of solid lipid nanoparticles to light may cause particle interaction and consequent gel network formation (36). In our particular case, the mixture of a lipid of high melting point (Compritol 888[®]) with one of low melting point (coconut fat) resulted in particles that were resistant on exposure to UVA at a temperature of 27–30°C. The use of Compritol 888[®] was based on its high melting point and chemical inertness, but the use of this solid lipid alone led to an unsuccessful *E*-RSV association. Thus, coconut fat was chosen as a solid lipid of lower melting point to be mixed with Compritol 888[®] because of earlier reports of its affinity with *E*-RSV (37).

Skin penetration

A combination of improved chemical stability of *E*-RSV and physical stability of the nanostructured system was used as the selection criteria. Lipid-core nanocapsules and NLC did not differ in terms of these two aspects and for this reason both particles were assayed to investigate *E*-RSV skin penetration.

The *E*-RSV was mostly concentrated in the dermis in all tests, confirming the high penetration capacity as described in a previous study (23). In the dark, the *E*-RSV penetration profile for lipid-core nanocapsules was similar to that for the free *E*-RSV, but in the case of the former there was a slight tendency toward lower drug concentrations in the viable epidermis and dermis. The NLC exhibited a lower concentration of *E*-RSV in the viable epidermis when compared to the free molecules in the dark. Under dark conditions, the association to a nanocarrier has little influence on the retention of *E*-RSV in the skin layers, resulting in no statistical differences. The maintenance of the penetration profiles of *E*-RSV from lipid-core nanocapsules and nanostructures' lipid carriers indicates that these formulations act as carriers and *E*-RSV is released from the structure and then penetrates the skin.

The use of a hydroalcoholic solution (40% vol/vol) was necessary to dissolve *E*-RSV at $1 \text{ mg}\cdot\text{mL}^{-1}$. Even though

ethanol is a permeability enhancer an decrease in skin deposition was not observed in dark conditions when compared the nanocarriers. A similar result was observed by Hung *et al.* (37), a 25% (vol/vol) hydroalcoholic solution had similar skin deposition value when compared with a pH 6 aqueous buffer.

When exposed to UVA radiation, application of the free molecule leads to higher quantities of *E*-RSV in the dermis and viable epidermis and lower quantities in the stratum corneum when compared with both nanostructures (lipid-core nanocapsules and NLC). Considering the total epidermis, the main site of action of topically applied antioxidants and chemopreventives, the nanostructures were capable of retaining the *E*-RSV.

The horny layer functions as a reservoir for topically applied drug, for this reason the interaction between the substance and the stratum corneum is very relevant for topical activity (38). The stratum corneum serves as the principal barrier for many molecules, but not for nonionic *E*-RSV (23). Although Hung *et al.* (37) observed that the stratum corneum did not serve as a barrier for RSV, under UVA radiation we demonstrated that lipid-core nanocapsules and nanostructured lipid carriers enhance the retention of RSV in the stratum corneum.

The higher quantities of *E*-RSV in the dermis after the application of the free molecule under irradiation also indicate that lipid-core nanocapsules and NLC promote retention of the active substance in the stratum corneum and on the surface of the skin preventing its accumulation in the dermis.

The application of free *E*-RSV resulted in low concentrations in the stratum corneum, probably due to a combination of UVA-induced degradation and skin retention. The lower quantities of the molecule in the upper layers, when compared to the values observed under dark conditions, resulted in lower concentrations in the dermis. The difference between the dermis and the total epidermis was much greater for the experiment with UVA exposure for all samples because a greater amount of UVA radiation reaches the upper layers (epidermis) when compared with deeper skin layers (dermis; 39) leading to less degradation of the molecule in the latter.

In conclusion, *E*-RSV presented first-order isomerization kinetics, which was maintained in all nanoparticle formulations. The nanostructures were capable of enhancing the *E*-RSV chemical photostability. Nanospheres were the particles that least protected *E*-RSV from photoisomerization. Lipid-core nanocapsules and NLC had the same isomerization rate and the liposomes were the particles that most protected *E*-RSV from photoisomerization. On the other hand, liposomes presented a poor physical stability, resulting in a bimodal size distribution profile. Considering the chemical and physical stability, lipid-core nanocapsules and NLC were the most adequate formulations for future pharmaceutical application. Lipid-core nanocapsules and NLC presented similar penetration profiles under dark conditions and on exposure to UVA radiation. When exposed to UVA radiation the *E*-RSV loaded nanocarriers led to higher concentrations of *E*-RSV in the total epidermis confirming that these particles are capable of reducing the high penetration characteristic of *E*-RSV.

Acknowledgements—This work was supported by the following Brazilian government agencies: Conselho Nacional de Desenvolvimento Científico e Tecnológico (CNPq), Coordenação de Aperfeiçoamento de Pessoal de Nível Superior (CAPES), Fundação de Amparo à Pesquisa do Estado do Rio Grande do Sul (FAPERGS) and Programa de Apoio a Núcleos de Excelência (PRONEX-CNPq/FAPERGS).

REFERENCES

- Sapino, S., M. E. Carlotti, G. Caron, E. Ugazio and R. Cavalli (2009) In silico design, photostability and biological properties of the complex resveratrol/hydroxypropyl- β -cyclodextrin. *J. Incl. Phenom. Macrocycl. Chem.* **63**, 171–180.
- Stivala, L. A., M. Savio, F. Carafoli, P. Perucca, L. Bianchi, G. Maga, L. Forti, U. M. Pagnoni, A. Albinii, E. Prosperi and V. Vannini (2001) Specific structural determinants are responsible for the antioxidant activity and the cell cycle effects of resveratrol. *J. Biol. Chem.* **276**, 22586–22594.
- Athar, M., J. H. Back, X. Tang, K. Ho Kim, L. Kopelovich, D. R. Bickers and A. L. Kim (2007) Resveratrol: a review of preclinical studies for human cancer prevention. *Toxicol. Appl. Pharm.* **224**, 274–283.
- Aziz, M. H., F. Afaq and N. Ahmad (2005) Prevention of ultraviolet-B radiation damage by resveratrol in mouse skin is mediated *via* modulation in survivin. *Photochem. Photobiol.* **81**, 25–31.
- Afaq, F., V. M. Adhami and N. Ahmad (2003) Prevention of short-term ultraviolet B radiation-mediated damages by resveratrol in SKH-1 hairless mice. *Toxicol. Appl. Pharmacol.* **186**, 28–37.
- Kalra, N., P. Roy, S. Prasad and Y. Shukla (2008) Resveratrol induces apoptosis involving mitochondrial pathways in mouse skin tumorigenesis. *Life Sci.* **82**, 348–358.
- Niles, R. M., M. McFarland, M. B. Weimer, A. Redkar, Y.-M. Fu and G. Meadows (2003) Resveratrol is a potent inducer of apoptosis in human melanoma cells. *Cancer Lett.* **190**, 157–163.
- Weiss-Angeli, V., F. S. Poletto, L. R. Zancan and F. Baldasso (2008) Nanocapsules of octyl methoxycinnamate containing quercetin delayed the photodegradation of both components under ultraviolet A radiation. *J. Biomed. Nanotechnol.* **4**, 80–89.
- Fontana, M. C., K. Coradini, A. R. Pohlmann, S. S. Guterres and R. C. R. Beck (2010) Nanocapsules prepared from amorphous polyesters: effect on the physicochemical characteristics, drug release, and photostability. *J. Nanosci. Nanotechnol.* **10**, 3091–3099.
- Ourique, A. F., A. R. Pohlmann, S. S. Guterres and R. C. R. Beck (2008) Rapid communication Tretinoin-loaded nanocapsules: preparation, physicochemical characterization, and photostability study. *Int. J. Pharm.* **352**, 1–4.
- Ioele, G., E. Cione, A. Risoli, G. Genchi and G. Ragno (2005) Accelerated photostability study of tretinoin and isotretinoin liposome formulations. *Int. J. Pharm.* **293**, 251–260.
- Schaffazick, S. R., S. S. Guterres, L. L. Freitas and A. R. Pohlmann (2003) Physicochemical characterization and stability of the polymeric nanoparticle system for drug administration. *Quim. Nova*, **26**, 726–737. (Portuguese)
- Mora-Huertas, C. E., H. Fessi and A. Elaissari (2010) Polymer-based nanocapsules for drug delivery. *Int. J. Pharm.* **385**, 113–142.
- Muller, R. H., K. Mader and S. Gohla (2000) Solid lipid nanoparticles (SLN) for controlled drug delivery—a review of the state of the art. *Eur. J. Pharm. Biopharm.* **50**, 161–177.
- Ourique, A. F., S. Azoubel, C. V. Ferreira, C. B. Silva, M. C. L. Marchiori, A. R. Pohlmann, S. S. Guterres and R. C. R. Beck (2010) Lipid-core nanocapsules as a nanomedicine for parenteral administration of tretinoin: development and *in vitro* antitumor activity on human myeloid leukaemia cells. *J. Biomed. Nanotechnol.* **6**, 1–10.
- Paese, K., A. Jäger, F. S. Poletto, E. Fonseca Pinto, B. Rossi-Bergmann, A. R. Pohlmann and S. S. Guterres (2009) Semisolid formulation containing a nanoencapsulated sunscreen: effectiveness, *in vitro* photostability and immune response. *J. Biomed. Nanotechnol.* **5**, 1–7.

17. Frozza, R., A. L. Bernardi, K. Paese, J. B. Hoppe, T. da Silva, A. M. O. Battastini, A. R. Pohlmann, S. S. Guterres and C. Salbego (2010) Characterization of *trans*-resveratrol-loaded lipid-core nanocapsules and tissue distribution studies in rats. *J. Biomed. Nanotechnol.* **6**, 694–703.
18. Ragno, G., E. Cione, A. Garofalo, G. Genchi, G. Ioele, A. Risoli and A. Spagnoletta (2003) Design and monitoring of photostability systems for amlodipine dosage forms. *Int. J. Pharm.* **265**, 125–132.
19. Mehnert, W. and K. Mäder (2001) Solid lipid nanoparticles production, characterization and applications. *Adv. Drug Deliv. Rev.* **47**, 165–196.
20. Shah, K. A., A. A. Date, M. D. Joshi and V. B. Patravale (2007) Solid lipid nanoparticles (SLN) of tretinoin: potential in topical delivery. *Int. J. Pharm.* **345**, 163–171.
21. Barnadas-Rodríguez, R. and M. Sabés (2001) Factors involved in the production of liposomes with a high-pressure homogenizer. *Int. J. Pharm.* **213**, 175–186.
22. Jager, A., V. Stefani, S. S. Guterres and A. R. Pohlmann (2007) Physico-chemical characterization of nanocapsule polymeric wall using fluorescent benzazole probes. *Int. J. Pharm.* **338**, 297–305.
23. Hung, C.-F., Y.-K. Lin, Z.-R. Huang and J.-Y. Fang (2008) Delivery of resveratrol, a red wine polyphenol, from solutions and hydrogels via the skin. *Biol. Pharm. Bull.* **31**, 955–962.
24. Guterres, S. S., M. P. Alves and A. R. Pohlmann (2007) Polymeric nanoparticles, nanospheres and nanocapsules, for cutaneous applications. *Drug Target Insights* **2**, 147–157.
25. Puglia, C., F. Bonina, F. Castelli, D. Micieli and M. D. Sarpietro (2009) Evaluation of percutaneous absorption of the repellent diethyltoluamide and the sunscreen ethylhexyl *p*-methoxycinnamate-loaded solid lipid nanoparticles: an *in vitro* study. *J. Pharm. Pharmacol.* **61**, 1013–1019.
26. Duncan, K. O., J. K. Geisse and D. J. Leffell (2008) Epithelial precancerous lesions. In *Fitzpatrick's Dermatology in General Medicine* (Edited by K. Wolff, L. A. Goldsmith, S. I. Katz, B. A. Gilchrest, A. S. Paller and D. L. Leffell), pp. 1007–1027. McGraw-Hill Companies, New York, NY.
27. Kristl, J., K. Teskac, C. Caddeo, Z. Abramović and M. Šentjurc (2009) Improvements of cellular stress response on resveratrol in liposomes. *Eur. J. Pharm. Biopharm.* **73**, 253–259.
28. Teskac, K. and J. Kristl (2010) The evidence for solid lipid nanoparticles mediated cell uptake of resveratrol. *Int. J. Pharm.* **390**, 61–69.
29. Zattoni, A., E. L. Piccolomini, G. Torsi and P. Reschiglian (2003) Turbidimetric detection method in flow-assisted separation of dispersed samples. *Anal. Chem.* **75**, 6469–6477.
30. Camont, L., C.-H. Cottart, Y. Rhayem, V. Nivet-Antoine, R. Djelidi, F. Collin, J.-L. Beaudeau and D. Bonnefont-Rousselot (2009) Simple spectrophotometric assessment of the *trans*-/*cis*-resveratrol ratio in aqueous solutions. *Anal. Chim. Acta* **634**, 121–128.
31. Kang, K. C., C.-I. I. Lee, H.-B. Pyo and N.-H. Jeong (2005) Preparation and characterization of nano-liposomes using phosphatidylcholine. *J. Ind. Eng. Chem.* **11**, 847–851.
32. Pardeike, J., A. Hommoss and R. H. Müller (2009) Lipid nanoparticles (SLN, NLC) in cosmetic and pharmaceutical dermal products. *Int. J. Pharm.* **366**, 170–184.
33. Mendonça, L. S., F. Firmino, J. N. Moreira, M. C. P. de Lima and S. Simões (2010) Transferrin receptor-targeted liposomes encapsulating anti-*BCR-ABL* siRNA or asODN for chronic myeloid leukemia treatment. *Bioconjug. Chem.* **21**, 157–168.
34. New, R. R. C. (1990) Characterization of liposomes. In *Liposomes: A Practical Approach* (Edited by R. R. C. New), pp. 113–117. Oxford University Press, New York, NY.
35. Alvarez-Lorenzo, C., L. Bromberg and A. Concheiro (2009) Light-sensitive intelligent drug delivery systems. *Photochem. Photobiol.* **85**, 848–860.
36. Heurtault, B., P. Saulnier, B. Pech, J.-E. Proust and J.-P. Benoit (2003) Physico-chemical stability of colloidal lipid particles. *Biomaterials* **24**, 4283–4300.
37. Hung, C.-F., C.-L. Fang, M.-H. Liao and J.-Y. Fang (2007) Pharmaceutical Nanotechnology the effect of oil components on the physicochemical properties and drug delivery of emulsions: Tocol emulsion versus lipid emulsion. *Int. J. Pharm.* **335**, 193–202.
38. Rougeire, A., D. Dupuis, C. Lotte, R. Roguet and H. Schaefer (1983) *In vivo* correlation between stratum corneum reservoir function and percutaneous absorption. *J. Invest. Dermatol.* **81**, 275–278.
39. UNEP/ICNIRP/WHO (1994) *Environmental Health Criteria 160, Health and Environmental Effects of Ultraviolet Radiation*. WHO, Geneva.